Tracer Penetration into Welded Tuff Matrix from Flowing Fractures

Qinhong Hu,* Timothy J. Kneafsey, Robert C. Trautz, and Joseph S. Y. Wang

ABSTRACT

Field and laboratory tracer experiments were conducted to investigate the extent of tracer imbibition and penetration into unsaturated, fractured rock matrix at Yucca Mountain, Nevada. Field experiments were carried out in the Exploratory Studies Facility (ESF), an underground tunnel at Yucca Mountain. Water containing dye was released into horizontal boreholes drilled into the wall of the ESF main drift. The region was then mined to observe the flow pathways and to collect dye-stained rock samples for subsequent laboratory quantification. Dye concentration profiles in the rock, measured using a newly developed sampling technique, showed that liquid flowing through the fractures penetrated into the matrix to a depth of several millimeters. Laboratory studies of tracer penetration into the rock matrix were conducted using tracer-free rock samples, collected from the same hydrogeologic unit and machined into cylindrical cores. Tracer-imbibition tests were performed on cores at two different initial water saturations with both sorbing (dyes) and nonsorbing tracers. The travel distance for sorbing dyes was a few millimeters after ~16 to 20 h, similar to the extent measured in samples from the field test. The nonsorbing bromide front coincided with the wetting front in the rock core at the initial water saturation of 12%, and the imbibition depth agreed very well with the prediction, using independently measured properties. At the high initial water saturation of 76%, the bromide front lagged significantly behind the wetting front. Sorption coefficients for the dyes in the partially saturated core samples were calculated using two independent approaches, based on tracer travel-distance and mass-distribution calculations, and were found to yield comparable results. Utilization of nonsorbing tracers with different molecular sizes helped to identify the effects of pore-size restriction on tracer transport during imbibition. The results from this work have a direct application to radionuclide transport at Yucca Mountain, and the methods presented are broadly applicable to the investigation of water and solute transport in unsaturated rock.

In low-permeability unsaturated fractured rock, water flows predominantly through the interconnected fracture network, with some water imbibing into the neighboring matrix rock. Imbibition (from the capillary pressure gradient) and diffusion (from the concentration gradient) drive mass transfer of solutes between the fractures and rock matrix. Imbibition and diffusion into the rock matrix can move contaminants away from the flowing fracture, thereby contributing to their retardation. Water flow in rock fractures and imbibition into the surrounding matrix in the unsaturated zone are key processes in evaluating the potential underground high-level radioactive waste repository at Yucca Mountain, Nevada.

A variety of conceptual models have been developed to describe flow and transport behavior in unsaturated fractured rock. In conventional continuum approaches based on volume-averaging concepts, liquid migration along subvertical fractures typically is predicted to be subject to strong matrix imbibition into the partially saturated rock (e.g., Wang and Narasimhan, 1993). Mounting evidence, however, points to the occurrence of fast and preferential flow, which suggests limited interaction of fractures with the surrounding matrix (Nativ et al., 1995; Glass et al., 1995; Yang et al., 1995; Tokunaga and Wan, 1997; Hu et al., 2001).

To explain the fast and preferential flow in unsaturated fractured rock, investigators have proposed models with different fracture–matrix interactions. Liu et al. (1998) presented an "active fracture model" in which only a portion of the connected fractures are active in conducting fluid in a steady-state flow field. Pruess (1999) proposed a mechanistic model that allowed water to flow relatively freely in networks of interconnected fractures despite strong suction from an unsaturated rock matrix; this model conceptualizes fracture flow as a spatially localized (within a fracture network) and transient (intermittent) process. However, Pruess noted that direct field observations remain incomplete. Field studies are required to directly estimate fracture–matrix interaction to calibrate or verify these conceptual models.

While fast and localized fracture flow has recently received broad acceptance, the importance of matrix imbibition and matrix flow in retarding contaminant migration should not be overlooked. The objective of this study was to investigate, through a combination of field and laboratory experiments, the spatial extent of matrix penetration by nonsorbing and sorbing tracers into fractured, unsaturated tuff. The purpose of the field tests was to observe the flow pathways; the purpose of the laboratory tests was to more completely quantify and understand tracer penetration into the tuff.

TRACER STUDIES IN FIELD FRACTURES

Field tests were conducted in two specially mined openings, called niches, located in the ESF. The niches are approximately 4 m wide, 3 m high, and 9 m deep within the Topopah Spring welded (TSw) volcanic tuff, the potential repository geologic unit. The intrinsic permeability for the rock matrix of the TSw is on the order of 10^{-18} m^2 (Flint, 1998). Figure 1 shows the location of seven horizontal boreholes installed at Niche 3650 (at the construction station 3650 m from the ESF North Portal) before the niche was excavated. The boreholes (0.076 m in diameter and ~10 m in length) were dry core-drilled. Three upper boreholes (UL, UM, and UR) were about 0.65 m above the top of the unmined niche. The remaining boreholes were drilled within the limits of the niche and were intentionally mined out when the niche was constructed. The configuration was similar for Niche 4788.

Liquid-release tests were conducted prior to the excavation

Q. Hu, T.J. Kneafsey, R.C. Trautz, and J.S.Y. Wang, 1 Cyclotron Road, MS 90-1116, Earth Sciences Division, Lawrence Berkeley National Laboratory, Berkeley, CA 94720. Received 15 Nov. 2001. *Corresponding author (q_hu@lbl.gov).

Published in Vadose Zone Journal 1:102–112 (2002).

Abbreviations: ESF, Exploratory Studies Facility; HPCD, hydroxypropyl-β-cyclodextrin; PFBA, pentafluorobenzoic acid; TSw, Topopah Spring welded [tuff].

of each niche. Water containing fluorescent or food dyes (Sulpho Rhodamine B or FD&C Blue No. 1) was pumped at a constant rate into 0.3-m-long test intervals isolated by a straddle packer system (Table 1). The maximum water level buildup within a test interval was 5 cm (Wang et al., 1999). The test intervals were more than 6 m into the rock from the borehole collar to minimize the boundary effects of the tunnel wall (e.g., drier matrix from the ventilation in the ESF). Generally, <1000 g of dye-laced water was introduced into each test interval. The niches were then mechanically dry-excavated within 7 to 13 d after the liquid release tests (Table 1). During excavation, the distribution of fractures and dye within the tuff was observed. Samples of the dye-stained rock were collected for subsequent laboratory analysis to profile dye penetration into the rock matrix from the flowing liquid through the fractures. Three rock samples from Niches 3650 and 4788 (Table 1) had dye stains on natural flat fracture faces and thus were selected for rock drilling. No visible fracture coating was observed for these three samples.

LABORATORY STUDIES

To quantify and understand imbibition into the tuff, we conducted laboratory tests to (i) examine tracer imbibition and penetration into the unsaturated rock matrix, (ii) evaluate the sample drilling and tracer profiling technique used for both laboratory and field samples, (iii) obtain the retardation factors for sorbing dyes in partially saturated core samples, and (iv) compare the fronts of imbibing water with those of nonsorbing bromide and sorbing dyes.

Water Imbibition and Tracer Penetration

Rock cores 5.08 cm in diameter and 2.0 cm in length were used to examine tracer imbibition and penetration by capillarity into the unsaturated rock matrix. Cores were cut and machined from a tracer-free sample block, collected at the construction station 4400 m within the same hydrogeologic unit as Niches 3650 and 4788. Porosity and bulk density were determined by weighing the sample (i) dried at 60°C, (ii) vacuum-saturated, and (iii) saturated and submerged (the method of Archimedes, Vennard and Street, 1975). This approach gives independent measurements of bulk density and porosity, with the measured porosity denoting the maximum rock void volume connected to the surface.

To investigate and compare tracer penetration behavior as a function of the initial water saturation level, we partially saturated cores by equilibrating them in relative humidity chambers controlled by different saturated brines or water until they reached constant weight. Cores with two different levels of initial water saturation (S_i), approximately 12 and 76%, were used in this work.

To simulate the imbibition and penetration of tracers into the rock matrix from a saturated fracture (a machined surface, in this case), we conducted tests by hanging the core from a balance inside a humidity-controlled chamber. The core bottom was submerged to a depth of about 1 mm in a tracer-containing solution (either Tracer Solution 1 or Tracer Solution 2). Sides of the core were coated with transparent epoxy, and the core top was loosely foil-covered, but left with a small hole for air escape. Epoxy was tested for water absorption by immersing it in water for 24 h, resulting in a 10% water gain, which accounts for only about 1.3% of the water storage capacity of air-dry rock cores. The imbibition rate was monitored by automatically recording the sample weight change over time. After a predetermined period of time (~16–20 h), the core was lifted out of the reservoir, and the position of the wetting front on the core sides was determined by visual inspection. Sampling for tracers was conducted immediately.

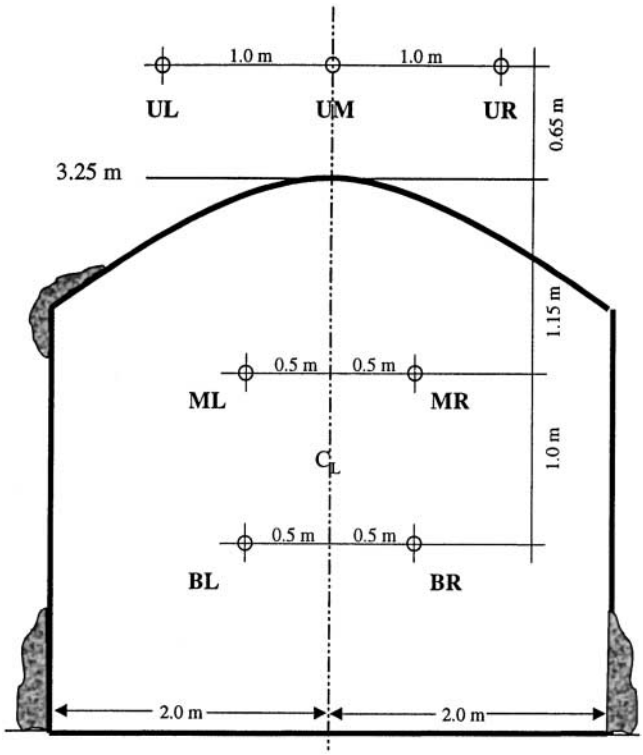

Fig. 1. Schematic of Niche 3650 end view (modified from Wang et al., 1999).

Tracer Solution 1 contained 10 g L^{-1} LiBr, 1 g L^{-1} FD&C Blue No. 1, and 1 g L^{-1} Sulpho Rhodamine B, which were selected to compare the behavior of the nonsorbing (bromide) and sorbing tracers (dyes and lithium). The sorbing dye tracers had been used in the field experiment. Tracer Solution 2 contained 10 g L^{-1} each of LiBr, pentafluorobenzoic acid (PFBA), and hydroxypropyl-β-cyclodextrin (HPCD). Solution 2 contained several nonsorbing tracers (bromide, PFBA, and HPCD) with different molecular sizes to investigate the potential effects of pore-size restriction and diffusion on tracer penetration during imbibition. Bromide has a reported value of 0.66 nm for its effective hydrated diameter (Nightingale, 1959), and HPCD has a molecular diameter of 1.5 nm (König, 1992).

Table 1. Compilation of information about the dye-stained rocks collected in the field.

Tracer	Test date	Test location§	Tracer conc.	Release rate	Release duration	Mass released	Sampling date
			g L^{-1}	mL s^{-1}	min	g	
Sulpho Rhodamine B†	8 Aug. 1997	ML 6.71–7.01 m	2.0	2.0	8.22	170.9	19 Aug. 1997
FD&C Blue No. 1†	6 Aug. 1997	UM 6.71–7.01 m	7.7	1.9	8.20	438.7	19 Aug. 1997
FD&C Blue No. 1‡	2 July 1998	UM 6.40–6.70 m	6.77	0.49	35.0	1019.7	9 July 1998

† Niche 3650.
‡ Niche 4788.
§ UM: upper middle borehole; ML: middle left borehole. Depth measurement (in meters) is from the collar of the boring to the test interval.

We are not aware of a reported molecular diameter for PFBA, but expect it to be about 0.7 nm, based on chemical structure and the reported diameter for similar molecules such as toluene (0.63 nm) and 1,3,5-trimethyl benzene (0.84 nm) (Satterfield et al., 1973). Average matrix pore diameters (weighted by pore space–filled increments) measured by mercury porosimetry are 53.1 nm and 19.7 to 21.4 nm for welded and densely welded tuff samples, respectively (Roberts and Lin, 1997). The reported aqueous diffusion coefficients (D_0) for bromide, PFBA, and HPCD are 2.08×10^{-9}, 7.89×10^{-10}, and 1.78×10^{-10} m^2 s^{-1}, respectively (Cussler, 1984; Hu and Brusseau, 1995).

Reagent-grade LiBr was purchased from EM Science (Gibbstown, NJ). FD&C Blue No. 1, with reported purity of 90% (Werner-Jenkinson Co., St. Louis, MO), was used without further treatment. Sulpho Rhodamine B (no purity reported) was obtained from Keystone Aniline Corp. (Santa Fe Springs, CA). PFBA (purity 99%) and HPCD (no purity reported) were purchased from Aldrich Chemical Co. (Milwaukee, WI), and 2-(*p*-toluidino)-naphthalene-6-sulfonic acid (TNS) (no purity reported) used for measuring HPCD was purchased from Sigma Chemicals (St. Louis, MO).

Rock Sampling and Tracer Extraction

A milling machine was used to drill a series of shallow holes at the same location in rock (either field or laboratory core) samples. Ten flat-bottom, carbide-end mill cutters with different diameters were used to drill to different depths. To minimize cross-contamination, the largest cutter size (19 mm) was used first to drill at the rock surface; subsequently smaller cutter sizes (the smallest being 14 mm) were used for increased drilling depth. No cutter was used for more than two intervals. Figure 2 shows an example of drill-sampled fracture rock. During drilling, a tube was placed around the cutter to reduce powder loss and maximize sample recovery. Drilling was carried out in 1-mm increments, as indicated by a Mitutoyo digital caliper with a precision of 0.01 mm.

The rock powder was collected for each 1-mm interval using a stainless-steel needle attached to a stainless-steel filter holder and connected to a vacuum source. Cellulose nitrate membranes (0.45-m pore size) inside the filter holder trapped the rock powder, which was vacuum-suctioned by pointing the needle to the drilled hole. Before drilling the subsequent intervals, we cleaned the hole with a gentle air stream to remove any residual powder, and the cutter with premoistened wipes, followed by drying with a gentle air stream. The collected powder passed through a sieve with a 104-mm opening.

For the three samples collected in the field, we conducted the rock drilling from the flat surface stained with a dye, since other sides were not smooth or not stained. Note that the field samples, though having a visually flat surface, are not expected to be as smooth as the machined cores, and the drilling depth is expected to have a small error. For the laboratory cores, we sampled the cylindrical cores from both the flat top (i.e., the core side not in direct contact with liquid) and bottom. We first drilled down from the top to a depth of 16 mm, and then inverted the core and drilled from the bottom to 10 mm deep. This sampling scheme allowed a comparison and evaluation of disturbance of tracer distribution potentially caused by the drilling method (discussed below). Drilling from the top and bottom was performed such that the drill holes did not intersect each other.

Dye tracers were extracted from the drill cuttings into the aqueous phase by mixing 0.1 g of the rock powder sample with 5 mL of Nanopure water (Barnstead, Dubuque, IA) in a glass tube with a vortex mixer for 15 s at a speed of 1400 rpm. The mixture was then filtered, and the concentration of the tracer in the aqueous phase was measured. Either Gelman Supor (Covina, CA) hydrophilic polyethersulfone membrane filters or Whatman (Clifton, NJ) cellulose-nitrate membranes were used for the filtration. Testing showed minimal mass loss of tracer to the membrane filters for FD&C Blue No. 1 and Sulpho Rhodamine B (about 95 ± 5% recovery).

Measurement of Aqueous Tracer Concentration

Aqueous concentration of FD&C Blue No. 1 was measured using a UV/Vis spectrophotometer (Model U-2001, Hitachi, Danbury, CT) at the characteristic wavelength of 630 nm. The Sulpho Rhodamine B concentration was measured using a fluorometer (Model RF-1501, Shimadzu Scientific, Columbia, MD) with excitation wavelength 565 nm and emission wavelength 590 nm. Analysis of HPCD was achieved by measuring the fluorescence of HPCD complexed with TNS (Brusseau et al., 1994) at the excitation wavelength of 300 nm and emission wavelength of 440 nm. Bromide concentration was measured by Ion Specific Electrode (Ionplus, Orion, Boston, MA), with the addition of an ionic strength adjuster at a volume ratio of 1:50. Background levels for all tracers were assessed using clean milled rock powder that passed through a 104-mm sieve.

We evaluated extraction efficiency by spiking a known amount of tracer into clean rock powder, allowing equilibration for 1 d, and following the identical extraction procedure. The results show the extraction efficiency (i.e., the ratio of recovered to spiked tracer mass) of 98.0 ± 4.6% (average ± standard deviation for 5 replicates) for bromide, 94.1 ± 3.8% for FD&C Blue No. 1 (6 replicates), and 88.2 ± 3.4% for Sulpho Rhodamine B (10 replicates). Tracer extraction efficiency was accounted for in the results presented below.

RESULTS AND DISCUSSION

Dye Penetration into Matrix from Field Fractures

Visual inspection of dyed rocks collected from the field studies showed that the dye stained the fracture surfaces. Color intensity decreased with distance into the matrix and disappeared within a few millimeters from the fracture surfaces into the rock. Figure 3 shows the measured concentration profile for a rock sample stained with the Sulpho Rhodamine B collected at Niche 3650. The depth on the x axis denotes the midpoint of drilling intervals; for example, the measured tracer concentration from the 1- to 2-mm drilling interval is shown at 1.5 mm. For the three field-collected rock samples stained with either FD&C Blue No. 1 or Sulpho Rhodamine B, the dye concentration decreased from the highest concentration to the background level in about 6 to 7 mm (Fig. 3, 4). These results show that water and tracer imbibition into the matrix from the liquid flowing through fractures occurred to a noticeable depth over the short experiment duration.

In conjunction with a gravity-driven liquid pulse through a fracture, the characteristic imbibition penetration depth, d, can be related to the time available for imbibition, t, derived by Zimmerman et al. (1995):

$$t = \frac{4\mu\phi\alpha n[m(S_s - S_r)]^{1/n}(V/A)^2(S_s - S_i)^m}{(n + 1)k} \qquad [1]$$

where μ is the viscosity of the pore water; ϕ is the matrix porosity; k is matrix permeability; α, m, and n are the

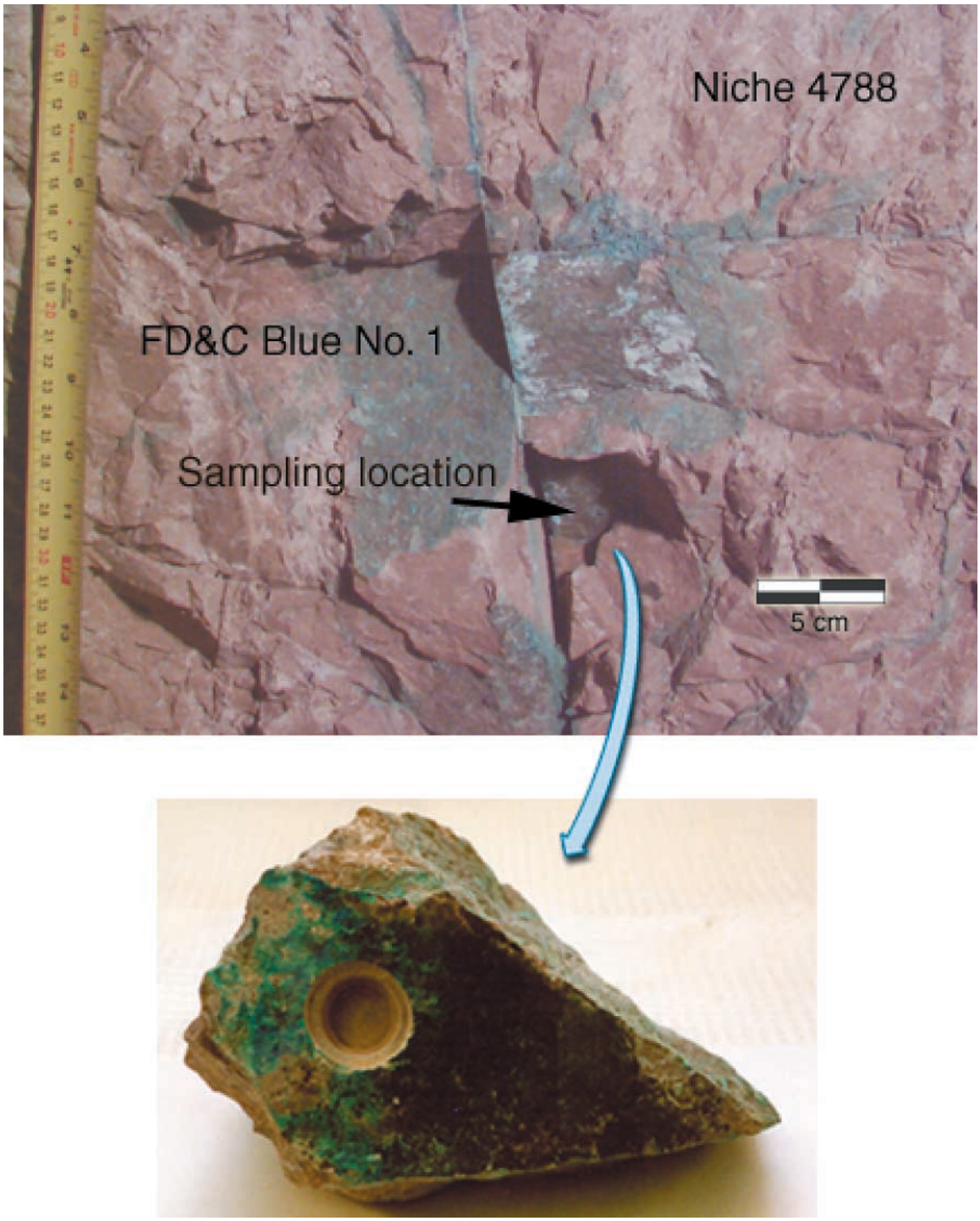

Fig. 2. Vertical view of the wall face showing the sampling location of rock (sample: Niche 4788) during niche excavation and example of drill-sampled fracture rock.

van Genuchten parameters (van Genuchten, 1980); and S_s, S_i, and S_r are saturated, initial, and residual saturation for the rock matrix, respectively. V is the volume and A the outer surface area of the matrix block, with the ratio of V to A the characteristic length scale of the matrix block. We assumed this to be d because no specific information about the geometry of the matrix block where field samples were collected is available. Using our measured matrix properties of cores ($\phi = 0.0877$, $\alpha = 7.8 \times 10^{-7}$ 1/Pa, $m = 0.353$, $n = 1.546$, $S_r = 0.022$, $k = 2.0 \times 10^{-19}$ m^2), $S_s = 1$, and $S_i = 0.85$ (in situ matrix saturation of 0.80–0.90, Flint, 1998), and $\mu = 10^{-3}$ Pa · s, the penetration depth of nonsorbing tracer (the effect of dye sorption on delayed transport will be discussed below) is estimated to be 1.5 mm for an imbibition time of 8.2 min for tracers released at Niche 3650 (Table 1). This estimate is in good agreement with the measured characteristic penetration depth, the distance to where

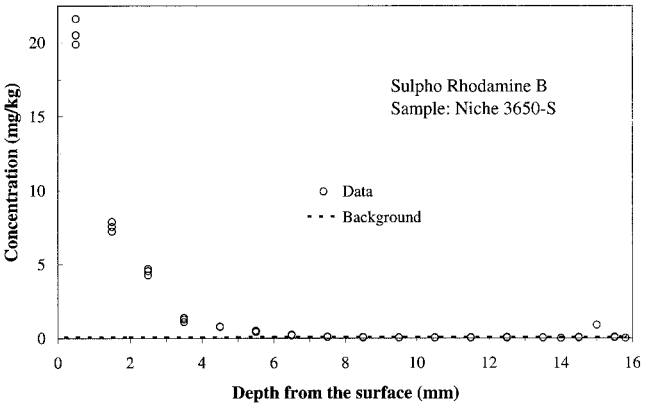

Fig. 3. Penetration profile of Sulpho Rhodamine B into the rock matrix from the fracture surface. Data shown are the measurement of three splits of the rock powder sample drilled at an interval.

the concentration is 50% of that at the fracture–matrix interface (0–1 mm interval in our case), which is about 1 to 2 mm for these two dyes. This comparison between theoretical and experimental imbibition assessment is quite encouraging and lends credence to the validity of Eq. [1] in estimating time scales for fracture–matrix and fracture–fracture flow, as discussed in Doughty (1999).

To compare the measured tracer concentration from dry rock (C_g, mg tracer g^{-1} rock) to the liquid tracer concentration on the volumetric basis (C_v, mg tracer cm^{-3} water), we use

$$C_v = \frac{C_g \rho_b}{\theta} \qquad [2]$$

with ρ_b the bulk density (g cm^{-3}) and θ the volumetric water content (cm^3 cm^{-3}) of the rock sample. The C_v value includes the tracer mass extracted from both the aqueous pore water and sorbed phases in the rock. In Eq. [2], we assume that the entire pore space was locally filled with tracer-bearing water when the tracer was deposited. With this conversion, the measured tracer concentration can be directly compared with the source concentration, C_0, to generate the C_v/C_0 value (Fig. 4).

The first few millimeters from the fracture surface contain the key portion of the tracer concentration profiles that indicate the extent of fracture–matrix interaction. Table 2 lists the tracer concentrations for the first millimeter (i.e., 0–1 mm from the fracture surfaces) for both field and laboratory core samples. Table 2 results represent a lower-bound value because the porosity is used as the volumetric water content, and total local saturation is not necessarily achieved. Moreover, the tracer release concentration of the test interval is used as tracer concentration in the flow through the fracture adjacent to the field samples. Actual tracer concentrations could be affected by water present in the fracture and losses resulting from sorption. In our calculations, we used mean measured bulk density (2.238 ± 0.029 g cm^{-3}) and porosity (0.0877 ± 0.009) values from 15 core samples obtained from the same hydrogeologic unit.

Table 2. Compilation of C_v/C_0 value at 0- to 1-mm interval from rock drilling.

Sample†	S_i(%)	Tracer	C_v/C_0(%)‡
Niche 3650-F	Not known	FD&C Blue No. 1	18.2 ± 0.5
Niche 3650-S	Not known	Sulpho Rhodamine B	26.4 ± 0.1
Niche 4788	Not known	FD&C Blue No. 1	112.1 ± 0.7
Core D	12.5	Bromide	140.9 ± 3.7
Core E	12.2	Bromide	137.9 ± 3.8
Core F	15.2	Bromide	110.9 ± 2.8
Core G	83.0	Bromide	93.3 ± 2.1
Core H	75.8	Bromide	109.3 ± 3.1
Core D	12.5	FD&C Blue No. 1	299.3 ± 1.9
Core H	75.8	FD&C Blue No. 1	234.1 ± 2.0
Core D	12.5	Sulpho Rhodamine B	308.6 ± 0.1
Core H	75.8	Sulpho Rhodamine B	308.0 ± 0.1

† Sample identification −F for tracer FD&C Blue No. 1 and −S for Sulpho Rhodamine B. Cores (D–H) were machined from a rock block of approximately 25 cm (length) by 15 cm (width) by 10 cm (height), collected from the construction station 4400 m of the ESF.

‡ Average of data ± background (measurements of three splits of the drilled rock powder).

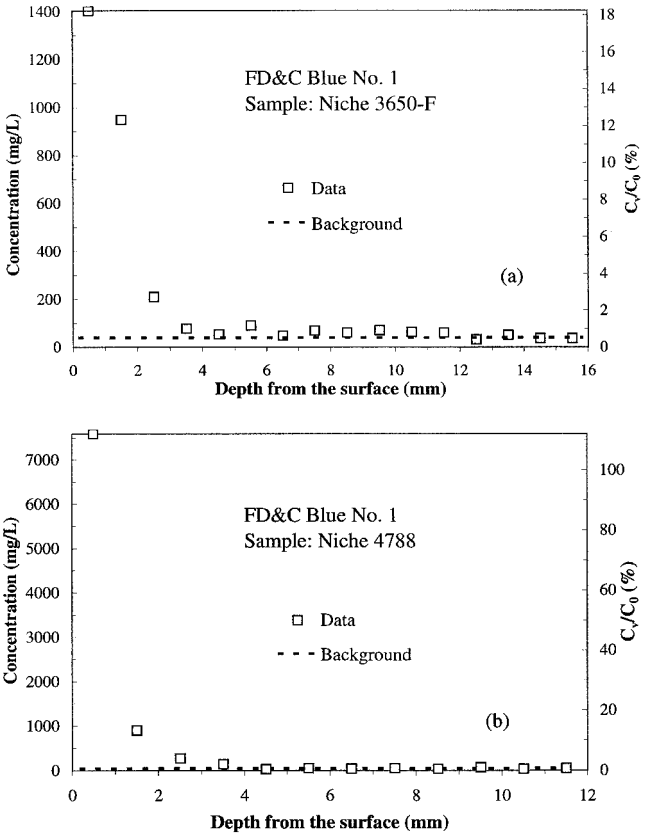

Fig. 4. Penetration profile of FD&C Blue No. 1, plotted as C_v and C_v/C_0, into the rock matrix from the fracture surface.

Samples Niche 3650-F and Niche 3650-S have concentration ratios C_v/C_0 of 18.2 and 26.4% for the first millimeter (Table 2). These relatively low values (compared with those obtained from laboratory Cores D and H to be discussed below) are associated with fast transient flows through the fractures. However, noticeable water and tracer imbibition into the matrix was observed, even though the fracture flow could have been fast.

In contrast, the C_v/C_0 in the first millimeter of the sample from Niche 4788 (see Fig. 4b and Table 2) was high. This sample was collected adjacent to a vertical flowing fracture that apparently dead-ended near the sampling location (Fig. 2). Figure 2 also shows the dye-stained flow pathways in a fracture network. High concentration in the first interval indicates greater imbibi-

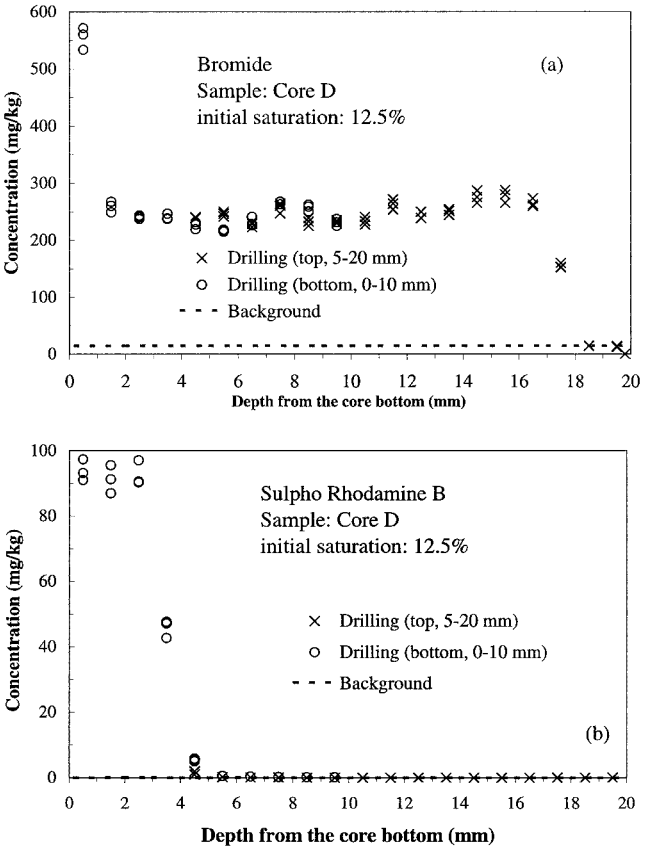

Fig. 5. Comparison of measured tracer concentrations from opposite drilling directions for Core D with S_i of 12.5%.

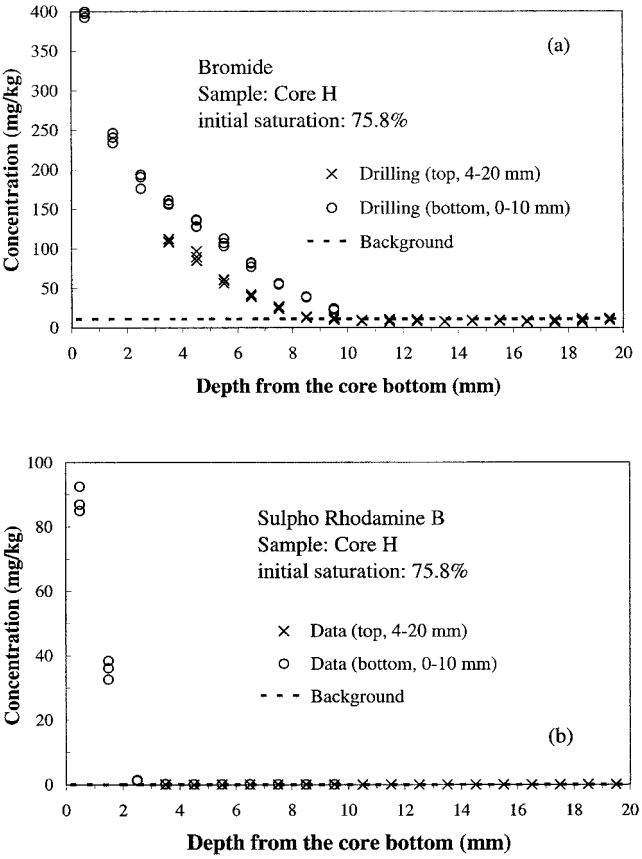

Fig. 6. Comparison of measured tracer concentrations from opposite drilling directions for Core H with S_i of 75.8%.

tion of the dye-spiked liquid, resulting from either a longer fluid–rock contact time (more likely) or a higher imbibition rate. The measured concentration ratio in the second interval (1–2 mm) drops steeply to 12.5%, similar to the other two field samples. A higher imbibition rate (related to such factors as an initially drier matrix) would have generated systematically higher concentration profiles at all intervals. Dye sorption into rock and its effect on matrix imbibition will be discussed in more detail below.

Evaluation of Core Drilling Technique

Alteration of tracer profiles during drilling was evaluated by drilling machined cores involved in imbibition experiments from both top and bottom. First, drilling was conducted 16 mm down from the core top, and then the core was inverted for drilling from the opposite side. In general, it took about 1 h to finish drilling and collecting samples for 10 depth intervals. Differences in concentrations for the two drilling directions could result from (i) gravitational flow during the second drilling phase, (ii) cross-contamination from powder carryover, (iii) sample heterogeneity, (iv) flow resulting from heating caused by drilling, and/or (v) flow resulting from evaporation caused by exposure to the atmosphere.

For both drilling directions, measured tracer concentrations vs. distance are shown in Fig. 5 and 6, with two different initial core saturations. For the low S_i case, the tracer concentration is comparable for both drilling directions (Fig. 5). Overall, the drilling technique yielded reliable concentration profile results, as indicated by the overlapping results for bromide (Fig. 5a). Only a slight difference at the 4- to 5-mm interval is observed for Sulpho Rhodamine B (Fig. 5b), even though its measurement had a very low detection limit of about 0.021 mg kg^{-1}.

For the case with the high S_i, the difference in measured concentration from the two drilling directions is noticeable, with bottom-drilled intervals having a higher concentration than top-drilled ones (Fig. 6a). Flow redistribution in the high S_i case (Fig. 6a) causes the difference to be more pronounced than the low S_i case, which has a steep tracer front (Fig. 5a). For Sulpho Rhodamine B, the apparent lack of change reflects its sorption and shorter travel distance (Fig. 6b). Tracer measurement results from the core top (when available) were utilized in the later discussion because they were performed first and were less susceptible to alteration. For field results, drilling proceeded only from the stained surface inward. Since these samples were air-dried when drilled, dye redistribution assisted by fluid flow during sampling (as shown in Core H) was not expected to significantly affect the dye distribution pattern.

Dye Sorption in Unsaturated Cores

Figure 7 provides a comparison between the concentration profiles of nonsorbing bromide and dyes, as well

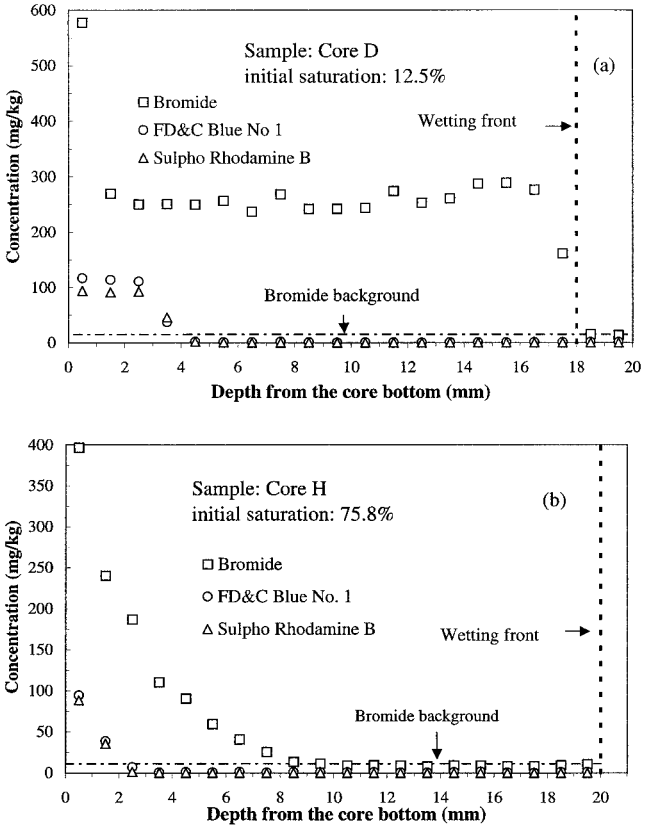

Fig. 7. Comparison of concentration profiles for the tracers: (a) Core D at the experimental duration of 19.5 h; (b) Core H at the experimental duration of 17.9 h.

as the wetting fronts determined by visual inspection. The dyes lag behind the bromide front, indicating dye sorption. FD&C Blue No. 1 and Sulpho Rhodamine B were the most visible dyes, making them very useful for flow pathway observation during niche excavation. These dyes have also been employed as tracers in numerous other studies (e.g., Smart and Laidlaw, 1977; Smettem and Trudgill, 1983; Flury and Fluhler, 1995; Perillo et al., 1998). Though they are negatively charged at normal pH, sorption of these dyes on rock is not surprising, considering their complex chemical structure with various functional groups. Sorption in soils for FD&C Blue No. 1 (Flury and Fluhler, 1995; Perillo et al., 1998) and for Sulpho Rhodamine B (Smettem and Trudgill, 1983) has been reported.

We can derive a retardation factor (R) at the end of the tracer-imbibition experiment from the travel distance of a nonsorbing tracer divided by that of a sorbing tracer. Retardation is important in that it will have the net effect of slowing radionuclide transport at Yucca Mountain. Because of its importance, we look at different ways to calculate it from our data. Bromide is found to be nonreactive with tuff from a column transport study (not presented), as well as indicated by its nearly coincident front with the wetting front at low S_i (Fig. 7a). In Fig. 7a, the bromide front is located at 17 to 18 mm from the core bottom ($d_{0.5}$ = 17.5 mm, with $d_{0.5}$ the distance at which the tracer concentration is half of the maximum concentration in the profile). For this evaluation, the first bromide data point at the 0- to 1-mm interval was treated as an outlier and was excluded from bromide front determination. Similar behavior was also noticed for other nonsorbing tracers (i.e., PFBA and HPCD). This inlet-end effect, to be further discussed below, did not seem to affect the sorbing dyes (probably because of the strong chemical sorption effect), as evident in the steady-state concentration of the first three intervals in Core D (Fig. 7a). For sorbing tracers, FD&C Blue No. 1 and Sulpho Rhodamine B, $d_{0.5}$ is about 3.5 mm (Fig. 7a). Therefore, the R value for both dyes is 5 (17.5 mm/3.5 mm) in Core D with S_i of 12.5%. Similarly, R is about 2.8 (3.5 mm/1.25 mm) for both dyes in Core H (Fig. 7b) with S_i of 75.8%.

In the transient imbibition process, the retardation factor is a function of water content that changes over time, while the sorption distribution coefficient, K_d, has been traditionally assumed to be independent of water saturation. The value of R is related to K_d by:

$$R = 1 + \frac{K_d \rho_b}{\theta} \qquad [3]$$

with K_d (mL g^{-1}) representing the distribution of solutes between aqueous and solid phase. This equation indicates that solute retardation is inversely related to the water content. Note that the concept of K_d implicitly denotes a linear equilibrium sorption behavior (e.g., Fetter, 1993). If the effective θ value is estimated as the average of the initial and the final water contents behind the wetting front, the K_d value can be derived from the R obtained above. We used the porosity as the final water content, although we realize the water content would be less due to air entrapment. The K_d values were calculated to be 0.089 mL g^{-1} for Core D and 0.063 mL g^{-1} for Core H. The measured bulk density and porosity values for each core were used in the calculations.

The value of K_d for each drilled interval can also be derived from mass-balance considerations:

$$K_d = \frac{C_g}{C_{pw}} - \frac{\theta}{\rho_b} \qquad [4]$$

where C_{pw} (mg L^{-1}) is the pore-water tracer concentration. For the inlet-end interval, the value of C_{pw} is assumed to be the same as that in the reservoir tracer solution. This interval was continuously in contact with the tracer reservoir (i.e., similar to a batch sorption experiment) allowing an equilibrium distribution of dyes between aqueous and solid phases. Using measured core porosity for water content θ (this interval is probably close to full saturation), we obtain K_d values similar to those calculated above (Table 3).

The retardation could also be viewed as the solute mass distribution among aqueous and solid phases. Substituting Eq. [2] and [3] into Eq. [4], we obtain (Shackelford, 1991):

$$R = \frac{C_v}{C_0} \qquad [5]$$

Therefore, the C_v/C_0 ratio in Table 2 directly denotes the extent of dye retardation for the inlet end from

Table 3. Measured K_d value (mL g^{-1}) by two approaches for dyes in two cores.

	Core D†			Core H	
Tracer	**Travel front**	**Travel front‡**	**Mass balance§**	**Travel front**	**Mass balance**
Bromide	–	–	0.016	–	0.003
FD&C Blue No. 1	0.089	0.059	0.079	0.063	0.054
Sulpho Rhodamine B	0.089	0.059	0.082	0.063	0.083

† Travel front approach assumes that bromide behaves as nonsorbing tracer, on which the K_d value for sorbing dyes is calculated.
‡ Calculated by taking into account of the average percentage (62%) of porosity that is conducting flow.
§ The K_d values from 0- to 1-mm interval by mass balance approach; data for bromide is for reference only as the boundary effect was noticed for nonsorbing tracers.

which an equilibrium K_d can be calculated (Table 3). Figure 8 shows the measured tracer distribution and the C_v/C_0 ratio for Core D sample. The ratio value in the inlet-end interval is as large as three for dyes, indicating their sorption (a value of one for nonsorbing tracer) into the rock, because C_v includes both aqueous and sorbed dye (see discussion for Eq. [2]). The ratio seems to be not related to initial water saturation (likely because of the overwhelming chemical sorption effect than physical flow processes), as the value is similar for Cores D and H. The inlet-end effect for nonsorbing bromide will be discussed below.

The agreement between K_d estimates from both mass-balance and travel-front calculations in Table 3 supports the validity of the assumptions (i.e., linear sorption behavior, effective θ estimate) for the experimental systems. More importantly, it lends credence to using an unsaturated transport–sorption approach to generate the K_d values for intact rock. Most of the K_d values in the literature have been acquired by batch experiments using crushed rock, with the sample sizes chosen more or less arbitrarily and mainly for experimental convenience. Batch experiments are generally performed, moreover, under saturated conditions with large water/rock ratios. Use of crushed-rock samples and the large water/rock ratio may generate K_d values unrepresentative of in situ conditions in unsaturated rock (Hu and Wang, 2001). The unsaturated transport–sorption approach presented here will overcome these limitations. In addition, this approach is especially useful for K_d measurements of weak fluid–rock–contaminant interactions (e.g., $K_d < 0.1$ mL g^{-1}), such as those we have encountered in this study. For weakly sorbing solutes, batch sorption work can yield *negative* K_d values with a large variability, because the K_d value is calculated from the difference of two large numbers (initial and final aqueous concentration). For example, from batch tests in devitrified tuff, the K_d for Np, an important radionuclide, is reported to be -0.04 ± 0.2 mL g^{-1} (Triay et al., 1997).

Extent of Matrix Imbibition at Field Tests

The concentration ratio C_v/C_0 in the first 1-mm interval (last four entries in Table 2) for the laboratory-tested core samples ($S_i \approx 12$ and 76%) was considerably higher than the ratio for two dye-stained field samples (first two entries of Table 2). This lower concentration in the field samples is the result of less imbibition, because the amount of imbibition is related to initial saturation of the rock matrix and contact time. For the field samples, the initial saturation may have been high (80–90% for rock matrix, as reported in Flint, 1998) and contact time is low. In the field studies, we expect dye sorption into the tuff matrix similar to what we observed in the laboratory tests. To provide a measure of matrix imbibition, we exclude the contribution of dye sorption by dividing the concentration ratio for field samples by that for laboratory cores. Using an average concentration ratio C_v/C_0 (in Table 2) for FD&C Blue No. 1 or Sulpho Rhodamine B as the extent of dye sorption, we obtain a value of 6.8% for FD&C Blue No. 1 and 8.6% for Sulpho Rhodamine B, respectively (average 7.7%), for dyed rock samples from Niche 3650. This value represents the percentage of nonsorbing tracer imbibed into the first 1-mm interval of the matrix adjacent to the flowing fracture relative to the controlled laboratory experiments. In other words, it provides a measure of the extent of fracture–matrix interaction (relative to matrix imbibition for our experimental conditions) for

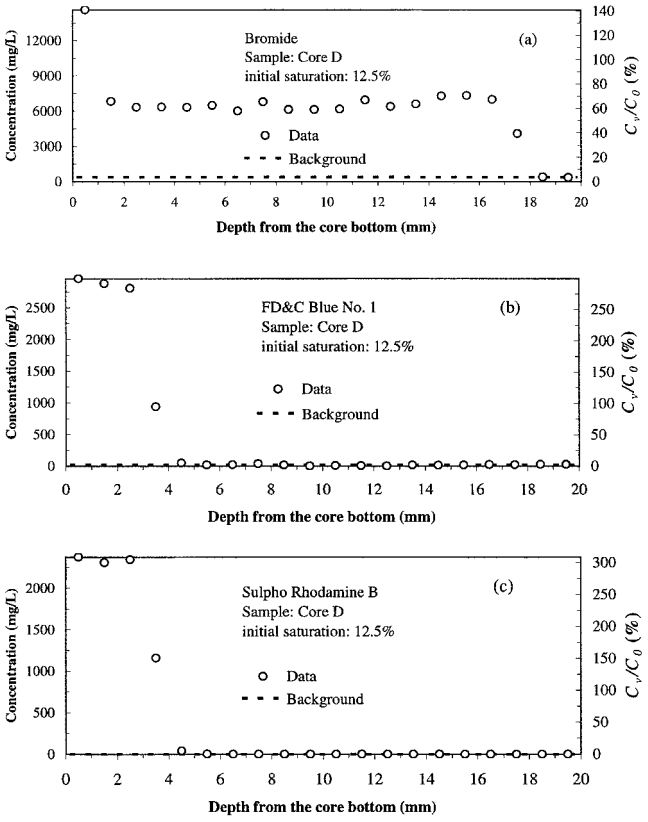

Fig. 8. Tracer penetration profile into the rock core matrix, plotted as C_v and C_v/C_0.

the fracture-dominated flow in the field relative to the laboratory experiments.

Dual-continuum models with a flow component between fractures and the matrix are used to model flow and transport in the unsaturated zone at Yucca Mountain. The fracture–matrix coupling term, however, is a poorly constrained parameter (Pruess et al., 1999). This work yields roughly 8% matrix-imbibition estimate (obtained from independent field and laboratory analyses) under field experimental conditions, which provides an important evaluation of the extent of matrix imbibition in the TSw unit of Yucca Mountain for a potential geological repository. This result indicates that matrix imbibition into relatively wet tuff matrix in situ can help delay contaminant transport to a measurable degree in conjunction with fast fracture flow. The extent of matrix imbibition is expected to be even larger in tuff matrix with relatively low initial saturation, which is expected to occur in disturbed conditions (e.g., ventilation and heating generated by nuclear waste).

For sorbing contaminants, the effect of matrix imbibition will be more pronounced, because this fracture–matrix flow provides the chance for these contaminants to contact the tuff matrix wherein sorption occurs. This enhanced delay for sorbing contaminants will also be augmented by the potential sorption onto fracture-coating materials, if such exist, in the flowing fractures. Most important radionuclides of concern are moderately to strongly sorbed to tuff matrix, with, for example, the average K_d values of about 1 mL g^{-1} for Np and U, and as large as 100 mL g^{-1} for Pu (Triay et al., 1997). Supposing a pulse of radionuclides is migrating downward through fractures, the retardation factor of Np or U, provided via matrix imbibition, will be as large as 30 in a rock matrix with 85% saturation, an in situ saturation under ambient steady-state flux. This will serve as an effective geologic barrier for the unsaturated rock.

Pore Connectivity and Tracer Front Characteristics

The average C_v/C_0 ratio from the five bromide tests at the inlet-end interval (0–1 mm) is 118 ± 20% for this nonsorbing (R = 100%) tracer (Table 2). The nonsorbing behavior of bromide was confirmed from column work using crushed tuff. The relatively large standard deviation likely results from the large liquid/solid ratio used in the extraction procedure, which magnifies inherent error when converted to tracer concentration. Noticeably, the steady-state bromide concentrations at low S_i measured at depth intervals between 1 and 16 mm are consistently at a C_v/C_0 ratio between 60 and 70% for Core D (shown in Fig. 8a) and 50 and 60% for Cores E and F. In other words, there is a high concentration (similar to the reservoir) at the inlet-end interval, and about 60% of measured total porosity participates in transport at the deeper intervals. If we use the effective porosity value as the water content behind the wetting front in calculating the K_d value from the travel-front approach, the K_d value is about 0.06 mL g^{-1} (Table 3).

The above observation of inlet-end effect is consistent with a network containing two kinds of pore systems, as explained by Ewing and Horton (2003): (i) a continuous pore system whose pores are accessible from each end and (ii) a discontinuous pore system whose pores can be reached from one end (the inlet end) but not the other. The discontinuous pore system only penetrates a small distance into the sample, but over this distance, the porosity available to solutes is greater than that deeper in the sample (i.e., the continuous pore system). The nonsorbing solute concentration in the inlet-end-only fraction will equilibrate with the reservoir concentration, given sufficient time.

For the imbibition experiment with low S_i (i.e., Core D), the bromide front is steep because a strong capillary force drives advective flow and tracer transport (Fig. 7a). During imbibition into a moist medium (i.e., Core H), solutes will disperse by mixing with "old" water, and so a less sharp profile of bromide is observed (Fig. 7b). In other words, dispersion becomes more pronounced for tracer transport under high S_i. In the infiltration tests with a sandy loam soil, Ghuman et al. (1975) also observed much more spreading for the chloride front in initially wet soil than in initially dry soil.

Bromide is frequently used for flow tracking. In rock core with a low S_i of 12.5%, the bromide front is comparable to the wetting front (Fig. 7a) that was visually observed to be located 18 mm away from the imbibition bottom. If we employ the same approach to describe characteristic imbibition depth for the field samples (Eq. [1]), we can predict that the wetting front will reach 19.1 mm after 19.5 h (compared with 18 mm from the likely conservative visual inspection) of experimental duration in this cylindrical core. The agreement between the experimental observation and prediction using all independently obtained parameters is quite encouraging.

In contrast with the coinciding fronts of bromide and moisture, the bromide front lags significantly behind the wetting front at the high S_i of 75.8% (Fig. 7b). The core top was observed to be wet at the end of the imbibition test. Under a high S_i, a relatively small amount of invading solution will push the antecedent water further ahead under transient flow. This front separation is consistent with the findings in moist soils (e.g., Warrick et al., 1971; Ghuman et al., 1975; Porro and Wierenga, 1993). The front separation must be considered seriously when using nonsorbing tracer to indicate the moisture movement in vadose studies. The extent of front separation will be very pronounced in low-porosity materials under high initial water saturations, such as the welded tuff under Yucca Mountain.

Effect of Tuff Pores on Tracer Imbibition

To further explore the potential contribution of diffusion and the effect of tuff pore sizes on imbibition, we employed three nonsorbing tracers with different molecular sizes and diffusivities (D_0) during imbibition into cores with two different water saturations. To take into account the different initial concentrations and the background levels of these tracers, we used the normal-

ized concentration to compare the results. The normalized concentration in the *y* axis of Fig. 9 is the ratio (measured concentration − background level)/(maximum measured concentration − background level).

In Core J with high S_i (83.0%), no effects are observed in the different tracers (Fig. 9a). The concentration profiles for bromide and HPCD are identical, even with the large difference in their D_0 values and molecular sizes, which indicates that diffusion is not an important component in the enhanced dispersion (i.e., mechanical dispersion is dominant). Furthermore, there is no restricted transport from steric hindrance in narrow pores for the sizes of tracer used. This is a reasonable observation because we expect that pores with equivalent diameters of less than about 2 μm will be filled with water during initial saturation in a well-controlled relative humidity chamber. The equivalent pore diameters for 83% initial saturation are estimated from the Kelvin equation and the Young–Laplace equation (Adamson, 1990).

In Core F with low S_i (15.2%), the concentration profiles from imbibition are different for bromide and HPCD (Fig. 9b). The profile for HPCD spreads more widely and also lags behind that for bromide, probably caused by the larger molecular size of HPCD. At this initial saturation, only the equivalent pore diameters less than about 25 nm were filled with water before the imbibition test. Therefore, imbibition of HPCD could be restricted from steric hindrance in small pores or narrow pore throats with diameters about one order of magnitude larger than the diffusant size (Grathwohl, 1998).

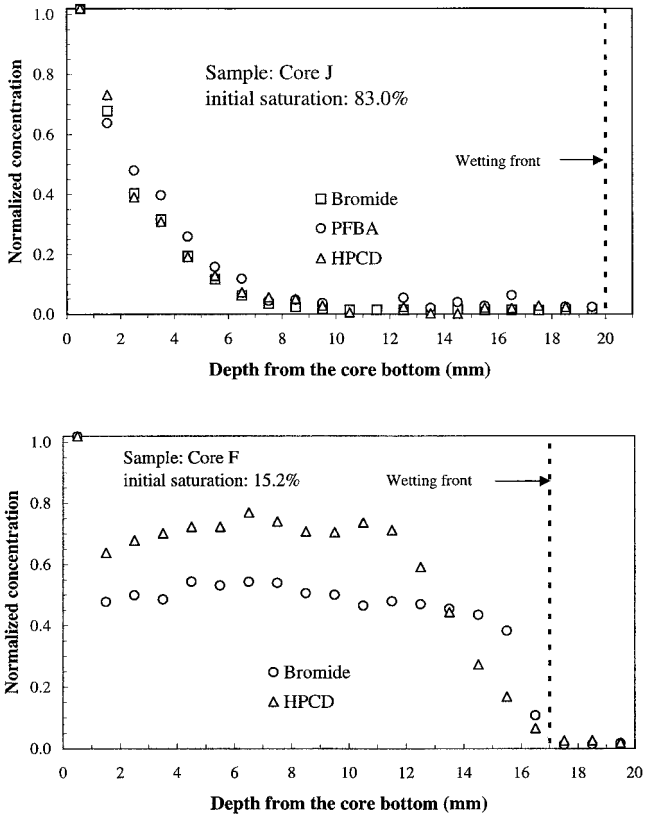

Fig. 9. Tracer penetration profile (plotted as the normalized concentration) into the rock core matrix: (a) Core J at the experimental duration of 16.1 h; (b) Core F at the experimental duration of 16.6 h.

SUMMARY AND CONCLUSIONS

Field and laboratory tracer experiments have been conducted to investigate the extent of fracture–matrix interaction and tracer penetration from fast fracture flow in unsaturated, fractured tuff. In the field tests, tracer-containing water was released at a specified interval within boreholes drilled along the ESF at the potential repository unit at Yucca Mountain. A niche was then mined to observe the flow pathways, and tracer-stained rock samples were collected for subsequent analyses. For laboratory studies, additional tracer-free tuff samples were machined into rock cores to study tracer penetration into the rock matrix under two initial water saturations. A drilling and sampling technique was developed to profile the tracer concentration in the rock matrix over distance. For field-collected rock samples, the sorbing dye tracer penetrated to depths of several millimeters into the matrix from fractures. In laboratory tracer-imbibition tests under both high and low initial water saturations, the concentration profiles of sorbing dyes lag behind the nonsorbing bromide front, with the travel distance for dyes a few millimeters over the contact time of about 16 to 20 h. Although bromide is not retarded by sorption, its front lags significantly behind the wetting front at high initial water saturation.

We showed that core measurements can be used to measure the extent of solute sorption using relatively large-sized unsaturated rock samples under flowing conditions. This unsaturated transport-sorption approach can be used to check the results commonly obtained from batch sorption experiments (which use saturated crushed tuff in static conditions), as well as to provide a more representative evaluation of sorption under field conditions.

Visibility makes dye tracers very useful for tracing water flow in geological media. Dyes used for field tests depict preferential flow pathways in the unsaturated fractured tuff and identify regions that have been in contact with flow in the fractures. Nevertheless, caution must be exercised when inferring water flow and solute transport from the sorbing dye results. Sorption of the dyes onto rock occurs because the dyes have complex chemical structure with various functional groups, even though both FD&C Blue No. 1 and Sulpho Rhodamine B are negatively charged under normal pH conditions. Moreover, tracer fronts (even for the nonsorbing tracers) do not necessarily coincide with the wetting fronts.

In the field experiments, we observed that matrix imbibition could remove ~8% of nonsorbing tracer from the flowing fracture into the first 1-mm interval of the matrix relative to our laboratory studies. We expect that this imbibition and consequent sorption of radionuclides into the rock matrix will contribute to the performance of a potential geological repository. Overall, results from combined field and laboratory efforts in the unsaturated, fractured low-permeability tuff at Yucca Moun-

tain provide direct evidence of predominant fracture flow and noticeable fracture–matrix interaction.

ACKNOWLEDGMENTS

This work was supported by the Director, Office of Civilian Radioactive Waste Management, U.S. Department of Energy, through Memorandum Purchase Order EA9013MC5X between Bechtel SAIC Company, LLC and the Ernest Orlando Lawrence Berkeley National Laboratory (Berkeley Lab). We thank Jil Geller, Peter Persoff, and Dan Hawkes of LBNL for many helpful comments. We also appreciate constructive comments from two anonymous reviewers.

REFERENCES

Adamson, A.W. 1990. Physical chemistry of surfaces. John Wiley and Sons, New York, NY.

Brusseau, M.L., X. Wang, and Q. Hu. 1994. Enhanced transport of low-polarity organic compounds through soil by cyclodextrin. Environ. Sci. Technol. 28:952–956.

Cussler, E.L. 1984. Diffusion: Mass transfer in fluid systems. Cambridge Univ. Press, New York, NY.

Doughty, C. 1999. Investigation of conceptual and numerical approaches for evaluating moisture, gas, chemical, and heat transport in fractured unsaturated rock. J. Contam. Hydrol. 38:69–106.

Ewing, R.P., and R. Horton. 2003. Diffusion scaling in low connectivity porous media. *In* Y. Pachepsky et al. (ed.) Bridging scales in soil physics. CRC Press, Boca Raton, FL. (In press.)

Fetter, C.W. 1993. Contaminant hydrogeology. Prentice Hall Inc., Upper Saddle River, NJ.

Flint, L.E. 1998. Characterization of hydrogeologic units using matrix properties, Yucca Mountain, Nevada. Water-Resources Investigations Report 97-4243. U.S. Geological Survey, Denver, CO.

Flury, M., and H. Fluhler. 1995 Tracer characteristics of brilliant blue FCF. Soil Sci. Soc. Am. J. 59:22–27.

Ghuman, B.S., S.M. Verma, and S.S. Prihar. 1975. Effect of application rate, initial soil wetness, and redistribution time on salt displacement by water. Soil Sci. Soc. Amer. Proc. 39:7–10.

Glass, R.J., M.J. Nicholl, and V.C. Tidwell. 1995. Challenging models for flow in unsaturated, fractured rock through exploration of small scale processes. Geophys. Res. Lett. 22:1457–1460.

Grathwohl, P. 1998. Diffusion in natural porous media: Contaminant transport, sorption/desorption and dissolution kinetics. Kluwer Academic Publishers, Boston, MA.

Hu, Q., and M.L. Brusseau. 1995. Effect of solute size on transport in structured porous media. Water Resour. Res. 31:1637–1646.

Hu, Q., R. Salve, W.T. Stringfellow, and J.S.Y. Wang. 2001. Field tracer transport tests in unsaturated fractured tuffs. J. Contam. Hydrol. 51: 1–12.

Hu, Q., and J.S.Y. Wang. 2001. Direct and high-resolution measurements of retardation and transport in whole rock samples under unsaturated conditions. American Geophysical Union, EOS Trans. 82(47):F501.

König, W.A.. 1992. Gas chromatographic enantiomer separation with modified cyclodextrins. Hüthig Verlag, Heidelberg, Germany.

Liu, H.H., C. Doughty, and G.S. Bodvarsson. 1998. An active fracture model for understanding unsaturated flow and transport in fractured rocks. Water Resour. Res. 34:2633–2646.

Nativ, R., E. Adar, O. Dahan, and M. Geyh. 1995. Water recharge and solute transport through the vadose zone of fractured chalk under desert conditions. Water Resour. Res. 31:253–261.

Nightingale, E.R., Jr. 1959. Phenomenological theory of ion solvation: Effective radii of hydrated ions. J. Phys. Chem. 63:1381–1387.

Perillo, C.A., S.C. Gupta, E.A. Nater, and J.F. Moncrief. 1998. Flow velocity effects on the retardation of FD&C Blue #1 food dye in soil. Soil Sci. Soc. Am. J. 62:39–45.

Porro, I., and P.J. Wierenga. 1993. Transient and steady-state transport through a large unsaturated soil column. Ground Water 31:193–200.

Pruess, K. 1999. A mechanistic model for water seepage through thick unsaturated zones in fractured rocks of low matrix permeability. Water Resour. Res. 35:1039–1051.

Pruess, K., B. Faybishenko, G.S. Bodvarsson. 1999. Alternative concepts and approaches for modeling flow and transport in thick unsaturated zones of fractured rocks. J. Contam. Hydrol. 38:281–322.

Roberts, J.R., and W. Lin. 1997. Electrical properties of partially saturated Topopah Spring tuff: Water distribution as a function of saturation. Water Resour. Res. 33:577–587.

Satterfield, C.N., C.K. Colton, and Pitcher, W.P., Jr. 1973. Restricted diffusion in liquid within fine pores. AIChE 19:628–635.

Shackelford, C. 1991. Laboratory diffusion testing for waste disposal—A review. J. Contam. Hydrol. 7:177–217.

Smart, P.L., and I.M.S. Laidlaw. 1977. An evaluation of some fluorescent dyes for water tracing. Water Resour. Res. 13:15–33.

Smettem, K.R.J., and S.T. Trudgill. 1983. An evaluation of some fluorescent and non-fluorescent dyes in the identification of water transmission routes in soils. J. Soil Sci. 34:45–56.

Tokunaga, T.K., and J. Wan. 1997. Water film flow along fracture surfaces of porous rock. Water Resour. Res. 33:1287–1295.

Triay, I.R., A. Meijer, J.L. Conca, K.S. Kung, R.S. Rundberg, B.A. Strietelmeier, and C.D. Tait. 1997. Summary and synthesis report on radionuclide retardation for the Yucca Mountain Site. Characterization Project Milestone 3784M. Los Alamos National Laboratory, Los Alamos, NM.

van Genuchten, M.Th. 1980. A closed-form equation for predicting the hydraulic conductivity of unsaturated soils. Soil Sci. Soc. Am. J. 44:892–898.

Vennard, J.K., and R.L. Street. 1975. Elementary fluid mechanics. 5th ed. John Wiley and Sons, Inc., New York, NY.

Wang, J.S.Y., and T.N. Narasimhan. 1993. Unsaturated flow in fractured porous media. *In* J. Bear et al. (ed.) Flow and contaminant transport in fractured rock. Academic Press, San Diego, CA.

Wang, J.S.Y., R.C. Trautz, P.J. Cook, S. Finsterle, A.L. James, and J. Birkholzer. 1999. Field tests and model analyses of seepage into drift. J. Contam. Hydrol. 38:323–347.

Warrick, A.W., J.W. Biggar, and D.R. Nielsen. 1971. Simultaneous solute and water transfer for an unsaturated soil. Water Resour. Res. 7:1216–1225.

Yang, I.C., G.W. Rattray, and P. Yu. 1995. Chemical and isotopic data and interpretations, unsaturated zone boreholes, Yucca Mountain, NV. Water Resources Investigation Report. U.S. Geological Survey, Denver, CO.

Zimmerman, R.W., T. Hadgu, and G.S. Bodvarsson. 1995. Transient dual-porosity simulations of unsaturated flow in fractured rocks. Report LBL-36807. Lawrence Berkeley National Laboratory, Berkeley, CA.